 CMES, vol.36, no.2, pp.97-117, 2008

Large Deformation Analysis with Galerkin based Smoothed Particle Hydrodynamics

S. Wong and Y. Shie

Abstract: In this paper, we propose a Galerkin-based smoothed particle hydrodynamics (SPH) formulation with moving least-squares meshless approximation, applied to solid mechanics and large deformation. Our method is truly meshless and based on Lagrangian kernel formulation and stabilized nodal integration. The performance of the methodology proposed is tested through various simulations, demonstrating the attractive ability of particle methods to handle severe distortions and complex phenomena.

Keyword: SPH, Galerkin method, large deformation

1 Introduction

The problems of computational mechanics grow ever more challenging. For example, in the simulation of manufacturing processes such as extrusion and molding, it is necessary to deal with extremely large deformations of the mesh while in computations of castings the propagation of interfaces between solids and liquids is crucial Onate, Idelson, Zienkievicz, and Taylor (1996); Idelsohn, Onate, and Pin (2004); Bonet and Kulasegaram (2000); Feldman and Bonet (2007); Khayyer and H. Gotoh (2008); Fang, Parriaux, Rentschler, and Ancey (in press); Antoci, Gallati, and Sibilla (2007); Wang, Lu, Hao, and Chong (2005). In simulations of failure processes, we need to model the propagation of cracks with arbitrary and complex paths. In the development of advanced materials, methods which can track the growth of phase boundaries and extensive microcracking are required Belytschko, Lu, and Gu (1995); Belytschko and Tabbara (1996); Organ, Fleming, Terry, and Belytschko (1996); Fleming, Chu, Moran, and Belytschko (1997); Hao, Liu, and Chang (2000); Liu, Hao, and Belytschko (1999); Hao and Liu (2006); Rabczuk and Belytschko (2006); Rabczuk and Zi (2007); Rabczuk, Areias, and Belytschko (2007b); Zi, Rabczuk, and Wall (2007); Ventura, Xu, and Belytschko (2002); Rabczuk and Belytschko (2004); Hao, Liu, Klein, and Rosakis (2004); Chandra and Shet (2004); Maiti and Geubelle (2004); Rabczuk, Areias, and Be-

lytschko (2007a); Rabczuk and Belytschko (2007); Nishioka, Kobayashi, and Fujimoto (2007); Hagihara, Tsunori, and Ikeda (2007); Guz, Menshykov, and Zozulya (2007); Guo and Nairn (2006); Rabczuk and Areias (2006); Gao, Liu, and Liu (2006); Fujimoto and Nishioka (2006); Nishioka (2005); Chen, Gan, and Chen (2008); Xu, Dong, and Zhang (2008); Wen, Aliabadi, and Lin (2008); Zhang and Chen (2008). These problems are not well suited to conventional computational methods such as finite element, finite volume or finite difference methods. The underlying structure of these methods which originates from their reliance on a mesh is not well suited to the treatment of discontinuities which do not coincide with the original mesh lines. Thus, the most viable strategy for dealing with moving discontinuities in methods based on meshes is to remesh in each step of the evolution so that mesh lines remain coincident with the discontinuities throughout the evolution of the problem. This can, of course, introduce numerous difficulties such as the need to project between meshes in successive stages of the problem, which lead to degradation of accuracy and complexity in the computer program, not to mention the burden associated with a large number of remeshings.

The objective of meshless methods is to eliminate at least part of this structure by constructing the approximation entirely in terms of nodes Atluri and Zhu (1998, 2000); Atluri and Shen (2002); Atluri (2002); Han and Atluri (2003); Tang, Shen, and Atluri (2003); Liu, Han, Rajendran, and Atluri (2006); Liu, Jun, and Zhang (1995a); Duarte and Oden (1996); Melenk and Babuska (1996); Belytschko, Lu, and Gu (1994a, 1995); Rabczuk and Belytschko (2005); Idelsohn and Onate (2006). Although in many meshless methods, recourse must be taken to meshes in at least parts of the method, moving discontinuities can usually be treated without remeshing with minor costs in accuracy degradation. Thus, it becomes possible to solve large classes of problems which are very awkward with mesh-based methods.

Since the early 1990s, research focus was devoted to meshless methods. The oldest meshless method is the Smoothed Particle Hydrodynamics (SPH) method developed in the late 1970s Lucy (1977). Improvements of this method flourished especially in the early 1990s Swegle, Hicks, and Attaway (1995); Monaghan (1994); Vignjevic, Campbell, and Libersky (2000); Liu, Jun, and Zhang (1995b); Bonet and Kulasegaram (2000); Krongauz and Belytschko (1997); Dilts (2000); Randles and Libersky (1997, 2000). SPH is method based on the strong form. It employs kernel function. Though many improvements were made, SPH and even many corrected SPH versions suffer from instabilities. Belytschko, Krongauz, Organ, Fleming, and Krysl (1996) showed that strong form based SPH can be regarded as weak formulation SPH using nodal integration and they showed instability due to under-integration. To overcome instability, stress-points were added to nodes Dyka and Ingel (1995). The stress points have to be relocated when the body undergoes

large deformations.

Another source of instability is connected to the kernel approximations. Eulerian kernel functions are commonly used in SPH formulations since typical application of SPH is for large deformations where Finite Element Method fails. However, Eulerian kernel functions often result in instabilities as demonstrated by Belytschko, Guo, Liu, and Xiao (2000). Lagrangian kernel functions can remove instabilities but limit the application of the method to moderate deformations Rabczuk, Belytschko, and Xiao (2004).

In this paper, we employ a SPH method to model problems with large deformations and damage in solid mechanics. Therefore, we interpret SPH as Galerkin method and use a stabilized nodal integration that removes instabilities. We do not need stress points that needs to be relocated when the body deforms. Updated Lagrangian kernel functions are used to eliminate other instability. Therefore, Lagrangian kernel functions are consequently updated. Hence, the method can handle large deformations. The method is applied to problems with severe distortions.

The paper is outlined as follows: We first state the governing equation. Then, we develop the SPH formulation and apply the method to some problems. At the end, we conclude our paper.

2 Governing Equations

In finite deformation analysis two possible co-ordinate systems can be chosen to describe the continuum under consideration [17, 18]. Lagrangian or material description is based on a certain reference configuration, that usually coincides with the initial configuration. Then, all relevant quantities are referred to a initial problem domain, Ω_0. The Eulerian or spatial description is based on the current continuum configuration. Here, relevant quantities are referred to the current problem domain, Ω. The former is most frequent in solid mechanics, whereas the latter is typical in fluid mechanics. These two descriptions will lead, in general, to non-equivalent discretizations in particle methods.

The governing equations solved in SPH method are the continuity equation, momentum equation and energy equation. Most SPH codes use an Eulerian rate form for mass conservation

$$\frac{d\rho}{dt} = -\rho div(\mathbf{v}) \tag{1}$$

where $d(\cdot)/dt$ denotes the material time derivative and $div(\mathbf{v})$ is computed in the current configuration. For a Lagrangian description, there is no need to use the Eulerian rate form, equation (1) and conservation of mass can be written in a material

form as an algebraic equation:

$$\rho J = \rho_0 \tag{2}$$

where ρ_0 and ρ are, respectively, the initial and current densities and J is the determinant of the deformation gradient, $J = det(\mathbf{F})$, $\mathbf{F} = \frac{d\mathbf{x}}{d\mathbf{X}} = \mathbf{I} - \frac{d\mathbf{u}}{d\mathbf{X}}$ where $\mathbf{I}$ is the second order unity tensor and $\mathbf{u}$ denotes the displacement field. In the following, $\mathbf{X}$, $\mathbf{x} = \mathbf{x}(\mathbf{X})$, ∇_X and ∇_x denote co-ordinates and gradient operators in the reference and current configurations, respectively.

In a Lagrangian description, conservation of linear momentum can be written as

$$\nabla_X \cdot \mathbf{P} + \mathbf{b} = \rho_0 \, \ddot{\mathbf{u}}, \quad \mathbf{X} \in \Omega_0 \tag{3}$$

where $\mathbf{b}$ is the body force per unit volume, superimposed dots denote material time derivatives and $\mathbf{P}$ is the first Piola-Kirchhoff stress tensor. Its Eulerian counterpart is

$$\nabla_x \cdot \sigma + \mathbf{b} = \rho \, \dot{\mathbf{v}}, \quad \mathbf{x} \in \Omega \tag{4}$$

where σ is the Cauchy stress tensor and ρ is the current density. The momentum equation can also be written in an arbitrary Lagrangian-Eulerian (ALE) form

$$\nabla_x \cdot \sigma + \mathbf{b} = \rho \left(\dot{\mathbf{v}} + \mathbf{v}^* \nabla_x \mathbf{v} \right), \quad \mathbf{x} \in \Omega \tag{5}$$

where $\mathbf{v}^*$ is the convective velocity. SPH-like particle methods follow the movement of a set of particles, so $\mathbf{v}^* = 0$ and the convective term in equation (5) vanishes. This is considered a Lagrangian description of the movement. When we say that (4) is posed in Eulerian form we mean that relevant quantities are referred to the current configuration, although the description is Lagrangian in the aforementioned sense.

Conservation of energy may also be considered in processes involving heat transfer or other related phenomena but we limit our studies to problems governed by equations (2) to (5).

Above field equations are complemented with displacement and traction boundary conditions that are given in the reference configuration:

$$\mathbf{u} = \bar{\mathbf{u}}, \quad \mathbf{X} \in \Gamma_{0u} \tag{6}$$

$$\mathbf{n}_0 \cdot \mathbf{P} = \mathbf{t}_0 = \bar{\mathbf{t}}_0, \quad \mathbf{X} \in \Gamma_{0t} \tag{7}$$

or in the current configuration

$$\mathbf{v} = \bar{\mathbf{v}}, \quad \mathbf{x} \in \Gamma_v \tag{8}$$

$$\mathbf{n} \cdot \sigma = \bar{\mathbf{t}}, \quad \mathbf{x} \in \Gamma_t \tag{9}$$

where the index t refers to traction boundaries, the index u refers to displacement boundaries and index v to imposed velocities; $\mathbf{n}$ is the normal to the traction boundary and the subscript 0 refers to quantities in the reference configuration.

3 SPH Method

The first SPH test and trial functions were given by

$$N_J(\mathbf{x}) = V_J W_J(\mathbf{x}) \tag{10}$$

where $W_J(\mathbf{x}) = W(\mathbf{x} - \mathbf{x}_J, h)$ is a kernel function with compact support centred at particle J and V_J is the tributary or statistical volume associated to particle J. The parameter h, usually called smoothing length or dilation parameter in the SPH literature is a certain characteristic measure of the size of the support of $W_J(\mathbf{x})$ (e.g. the radius in circular supports). Exponential and spline functions are most frequent kernels. We have not found a general criterion for an optimal choice and used the quartic spline function that is commonly used in the literature:

$$W(\mathbf{x}-\mathbf{x}_I, h) \quad = \quad w(s) = \begin{cases} 1-6s^2+8s^3-3s^4 & s \leq 1 \\ 0 & s > 1 \end{cases} \tag{11}$$

with $s = \frac{\mathbf{x}-\mathbf{x}_I}{2h}$ for circular support size.
The SPH approximation $\mathbf{u}^h(\mathbf{x})$ of a given function $\mathbf{u}(\mathbf{x})$ can be posed in terms of the shape functions, equation (10) and certain particle or nodal parameters $\mathbf{u}_J$ as

$$\mathbf{u}^h(\mathbf{x}) = \sum_{J=1}^{n} N_J(\mathbf{x})\mathbf{u}_J \tag{12}$$

with n numbers of neighboring particles with $N_J(\mathbf{x}) \neq 0$. Using standard kernels, the approximation given by equation (12) is poor near boundaries, and lacks even zeroth-order completeness

$$\sum_{J=1}^{n} N_J(\mathbf{x}) = 1 \tag{13}$$

Thus, the set $\{N_J(\mathbf{x}), J = 1, ..., n\}$ does not constitute a signed partition of unity Melenk and Babuska (1996); Duarte and Oden (1996). To eliminate this remedy, we adopt a correction of the SPH approximation that is based on Moving Least Squares (MLS) approximation. The MLS approximation is frequently used in meshfree methods such as the famous Meshless Local Petrov Galerkin (MLPG) method Atluri and Zhu (1998), the elementfree Galerkin (EFG)-method Belytschko, Lu, and Gu (1994b) and Moving Least Squares Particle Hydrodynamics (MLSPH)

Dilts (2000). In fact, it can be shown that the latter two methods are specific cases of the MLPG method.

The basic idea of the MLS approach is to approximate $\mathbf{u}(\mathbf{x})$, at a given point $\mathbf{x}$, through a polynomial least-squares fitting of $\mathbf{u}(\mathbf{x})$ in a neighbourhood of $\mathbf{x}$ as

$$\mathbf{u}^h(\mathbf{x}) = \sum_{I=1}^{m} p_I(\mathbf{x}) a_I(\mathbf{z})|_{\mathbf{z}=\mathbf{x}} = \mathbf{p}^T(\mathbf{x})\, \mathbf{a}(\mathbf{z})|_{\mathbf{z}=\mathbf{x}} \tag{14}$$

where $\mathbf{p}^T(\mathbf{x})$ is an m-dimensional polynomial basis and $\mathbf{a}(\mathbf{z})|_{\mathbf{z}=\mathbf{x}}$ is a set of parameters to be determined, such that they minimize the following error functional:

$$\mathscr{J}(\mathbf{a}(\mathbf{z})|_{\mathbf{z}=\mathbf{x}}) = \int_{\mathbf{y}\in\Omega_x} W(\mathbf{z}-\mathbf{y},h)|_{\mathbf{z}=\mathbf{x}} \left(\mathbf{u}(\mathbf{y}) - \mathbf{p}^T(\mathbf{y})\mathbf{a}(\mathbf{z})|_{\mathbf{z}=\mathbf{x}}\right) d\Omega_x \tag{15}$$

being $W(\mathbf{z}-\mathbf{y},h)|_{\mathbf{z}=\mathbf{x}}$ a symmetric kernel with compact support (denoted by Ω_x), frequently chosen among the kernels used in standard SPH. The stationary conditions of $\mathscr{J}$ with respect to $\mathbf{a}$ lead to

$$\int_{\mathbf{y}\in\Omega_x} \mathbf{p}(\mathbf{y}) W(\mathbf{z}-\mathbf{y},h)|_{\mathbf{z}=\mathbf{x}} \mathbf{u}(\mathbf{y})\, d\Omega_x = \mathbf{M}(\mathbf{x})\mathbf{a}(\mathbf{z})|_{\mathbf{z}=\mathbf{x}} \tag{16}$$

with moment matrix

$$\mathbf{M}(\mathbf{x}) = \int_{\mathbf{y}\in\Omega_x} \mathbf{p}(\mathbf{y}) W(\mathbf{z}-\mathbf{y},h)|_{\mathbf{z}=\mathbf{x}} \mathbf{p}^T(\mathbf{y})\, d\Omega_x \tag{17}$$

In numerical computations, the global domain Ω is discretized by a set of n particles. We can then evaluate the integrals in equations (16) and (17) using those particles inside Ω_x as quadrature points (nodal integration) to obtain, after rearranging,

$$\mathbf{a}(\mathbf{z})|_{\mathbf{z}=\mathbf{x}} = \mathbf{M}^{-1}(\mathbf{x})\mathbf{P}_{\Omega_x}\mathbf{W}(\mathbf{x})\mathbf{u}_{\Omega_x} \tag{18}$$

where the vector $\mathbf{u}_{\Omega_x}$ contains certain nodal parameters of those particles in Ω_x, the discrete version of $\mathbf{M}$ is $\mathbf{M}(\mathbf{x}) = \mathbf{P}_{\Omega_x}\mathbf{W}(\mathbf{x})\mathbf{P}_{\Omega_x}^T$, and matrices $\mathbf{P}_{\Omega_x}$ and $\mathbf{W}(\mathbf{x})$ can be obtained as

$$\mathbf{P}_{\Omega_x} = \{\mathbf{p}(\mathbf{x}_1), \mathbf{p}(\mathbf{x}_1), ..., \mathbf{p}(\mathbf{x}_n)\} \tag{19}$$

$$\mathbf{W}(\mathbf{x}) = diag\{W_I(\mathbf{x}-\mathbf{x}_I,h)V_I\},\ I = 1,...,n \tag{20}$$

where n denotes the total number of particles within the neighborhood of point $\mathbf{x}$ and V_I and $\mathbf{x}_I$ are, respectively, the tributary volume (used as quadrature weight) and co-ordinates associated to particle I.

Introducing equation (18) in equation (12) the interpolation structure can be identified as

$$\mathbf{u}^h(\mathbf{x}) = \mathbf{p}^T(\mathbf{x})\mathbf{M}^{-1}(\mathbf{x})\mathbf{P}_{\Omega_x}\mathbf{W}(\mathbf{x})\mathbf{u}_{\Omega_x} \tag{21}$$

Henceforth, the MLS shape functions are

$$\mathbf{N}^T(\mathbf{x}) = \mathbf{p}^T(\mathbf{x})\mathbf{M}^{-1}(\mathbf{x})\mathbf{P}_{\Omega_x}\mathbf{W}(\mathbf{x}) \tag{22}$$

Instead of the global polynomial basis $\mathbf{p}(\mathbf{y})$, we use a scaled locally defined polynomial basis $\mathbf{p}((\mathbf{y}-\mathbf{x})/h)$, that leads to better conditioned moment matrix $\mathbf{M}$. In this work, we use a linear polynomial basis

$$\mathbf{p}((\mathbf{y}-\mathbf{x})/h) = \{1,(y_1-x_1)/h,(y_2-x_2)/h\} \tag{23}$$

where (x_1,x_2) and (y_1,y_2) are, respectively, the Cartesian co-ordinates of $\mathbf{x}$ and $\mathbf{y}$. This guarantees linear completeness and constitutes a signed partition of unity method.

Finally, we remark that all derivations above are done equivalently for a Lagrangian description.

4 Discretization

The meshless discrete equations can be derived using a weighted residuals formulation. In the MLPG method, different test and trial functions are employed and a local weak form over local sub-domains is used. It is easy to show that due to the choice of local weak form, MLPG leads to truly meshless method Atluri and Zhu (1998), i.e. no background cells for integration are necessary as opposed to the EFG method that is based on the global weak form and therefore does not result in a truly meshless method since background mesh is needed to perform integration. Therefore, it is commonly referred to as semi-meshless method.

The discrete counterpart of the Galerkin weak form is almost equivalent to that obtained from kernel estimates Belytschko, Guo, Liu, and Xiao (2000); Beissel and Belytschko (1996) such as classical SPH formulations. Furthermore, such an equivalence indicates that SPH can be studied in the context of Galerkin methods. We employ a global weak form and use nodal integration that maintains the truly meshless character since no background mesh is needed for integration. However, nodal integration leads to instabilities that need to be corrected (see below for more details). The global weak (integral) form of the spatial momentum equation can be stated in Lagrangian formulation as: Find $\mathbf{u} \in \mathscr{U}$ and $\delta\mathbf{u} \in \mathscr{U}_0$ such that

$$\delta W = \delta W_{int} - \delta W_{ext} + \delta W_{kin} = 0 \tag{24}$$

with

$$\begin{aligned}
\delta W_{int} &= \int_{\Omega_0} \nabla_X \delta\mathbf{u} : \mathbf{P}\, d\Omega_0 \\
\delta W_{ext} &= \int_{\Gamma_{0t}} \delta\mathbf{u}\cdot\bar{\mathbf{t}}_0\, d\Gamma_0 + \int_{\Omega_0} \delta\mathbf{u}\cdot\mathbf{b}\, d\Omega_0 \\
\delta W_{kin} &= \int_{\Omega_0} \rho_0 \delta\mathbf{u}\cdot\ddot{\mathbf{u}}\, d\Omega_0
\end{aligned} \tag{25}$$

with the approximation spaces $\mathscr{U}$ and $\mathscr{U}_0$ for the trial and test functions, respectively,

$$\begin{aligned}
\mathscr{U} &= \left\{\mathbf{u} | \mathbf{u} \in H^1,\ \mathbf{u} = \bar{\mathbf{u}}\ on\ \Gamma_u\right\} \\
\mathscr{U}_0 &= \left\{\delta\mathbf{u} | \delta\mathbf{u} \in H^1,\ \delta\mathbf{u} = 0\ on\ \Gamma_u\right\}
\end{aligned} \tag{26}$$

For Eulerian description, we obtain similarly expressions

$$\begin{aligned}
\delta W_{int} &= \int_{\Omega} \nabla_x \delta\mathbf{v} : \sigma\, d\Omega \\
\delta W_{ext} &= \int_{\Gamma_t} \delta\mathbf{v}\cdot\bar{\mathbf{t}}\, d\Gamma + \int_{\Omega} \delta\mathbf{v}\cdot\mathbf{b}\, d\Omega \\
\delta W_{kin} &= \int_{\Omega} \rho\, \delta\mathbf{v}\cdot\dot{\mathbf{v}}\, d\Omega
\end{aligned} \tag{27}$$

with approximation spaces $\mathscr{V}$ and $\mathscr{V}_0$ for the trial and test functions, respectively:

$$\begin{aligned}
\mathscr{V} &= \left\{\mathbf{v} | \mathbf{v} \in H^1,\ \mathbf{v} = \bar{\mathbf{v}}\ on\ \Gamma_v\right\} \\
\mathscr{V}_0 &= \left\{\delta\mathbf{v} | \delta\mathbf{v} \in H^1,\ \delta\mathbf{v} = 0\ on\ \Gamma_v\right\}
\end{aligned} \tag{28}$$

The test and trial functions have the structure of equation (21). Introducing them into the weak formulation with a Bubnov Galerkin method yields

$$\sum_{I=1}^{n} \delta\mathbf{u}_I \left\{ \sum_{J=1}^{n} - \int_{\Omega_0} \nabla_X N_I(\mathbf{X})\mathbf{P}\, d\Omega_0 + \int_{\Omega_0} N_I(\mathbf{X})\mathbf{b}\, d\Omega_0 + \int_{\Gamma_{0t}} N_I(\mathbf{X})\bar{\mathbf{t}}_0\, d\Gamma_0 + \int_{\Omega_0} \rho_0 N_I(\mathbf{X}) N_J(\mathbf{X})\mathbf{u}\, d\Omega_0 \right\} = 0 \tag{29}$$

Thus, for each particle I, the following identity must hold

$$\sum_{J=1}^{n} \int_{\Omega_0} \nabla_X N_I(\mathbf{X})\mathbf{P}\, d\Omega_0 = \int_{\Omega_0} N_I(\mathbf{X})\mathbf{b}\, d\Omega_0 + \int_{\Gamma_{0t}} N_I(\mathbf{X})\bar{\mathbf{t}}_0\, d\Gamma_0 + \int_{\Omega_0} \rho_0 N_I(\mathbf{X}) N_J(\mathbf{X})\mathbf{u}\, d\Omega_0 = 0 \tag{30}$$

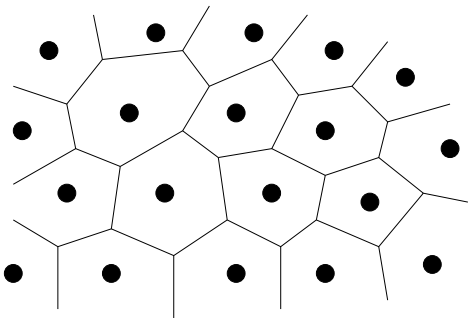

Figure 1: Voronoi cell diagram

The discrete equations for the Eulerian formulation look similar. These equations can be recast into a matrix form

$$\mathbf{M}_{IJ}\ddot{\mathbf{u}}_J = -\mathbf{f}_I^{ext} + \mathbf{f}_I^{int} \tag{31}$$

with

$$\mathbf{M}_{IJ} = \int_{\Omega_0} \rho \mathbf{N}_I(\mathbf{X})\, \mathbf{N}_J^T(\mathbf{X})\, d\Omega_0$$

$$\mathbf{f}_I^{ext} = \int_{\Gamma_{0t}} \mathbf{N}_I^T(\mathbf{X})\, \bar{\mathbf{t}}_0 d\Gamma_0 + \int_{\Omega_0} \mathbf{N}_I^T(\mathbf{X})\, \mathbf{b} d\Omega_0 \tag{32}$$

$$\mathbf{f}_I^{int} = \int_{\Omega_0} \nabla_X \mathbf{N}_I^T \mathbf{X})\, \mathbf{P} d\Omega_0 \tag{33}$$

Nodal integration has been used, at least implicitly, in all SPH formulations, and lies, indeed, in the basis of its early formulation. It is obviously the cheapest option and the resulting scheme is truly meshless. The particles are used as quadrature points and the corresponding integration weights are their tributary volumes:

$$\mathbf{M}_{IJ} = \sum_{K=1}^{n} \rho_K N_I(\mathbf{X}_K) N_J(\mathbf{X}_K) V_K \tag{34}$$

$$\mathbf{f}_I^{ext} = \sum_{K=1}^{n} \mathbf{N}_I^T(\mathbf{X}_K)\, \bar{\mathbf{b}}_K V_K + \sum_{K=1}^{n} \mathbf{N}_I^T(\mathbf{X}_K)\, \bar{\mathbf{t}}_{K0} A_K \tag{35}$$

$$\mathbf{f}_I^{int} = \sum_{K=1}^{n} \nabla_X \mathbf{N}_I^T \mathbf{X}_K) \, \mathbf{P}_K V_K \tag{36}$$

In the above, V_K represents the tributary volume associated to particle K. These volumes are obtained from Voronoi diagrams, figure 1. Hence, the particles are set up with certain initial densities, volumes and, therefore, masses. These physical masses M_K remain constant during the simulation and densities are field variables updated through an algebraic equation (2).

Since nodal integration is the origin of well-known instabilities in meshless methods, we introduce a strain smoothing stabilization that avoids these instabilities Chen, Wu, Yoon, and You (2001); You, Chen, and Voth (2002). Therefore, the strain tensor is transformed by Gauss' divergence theorem

$$\tilde{\varepsilon} = \int_{\Gamma_{V_K}} \frac{1}{V_K} (\mathbf{u} \otimes \mathbf{n} + \mathbf{n} \otimes \mathbf{u} \; d\Gamma) \tag{37}$$

where V_K is the volume of the Voronoi cell K, figure 1, and $\mathbf{n}$ is the normal to the cell K.

Large deformations are accounted for by computing nodal deformation gradients $\mathbf{F}$. Then the first Piola-Kirchoff stress $\mathbf{P}$ is used in place of the Cauchy stress tensor. For total Lagrangian, $\mathbf{X}$ refers to the undeformed reference configuration. For updated Lagrangian, $\mathbf{X}$ refers to some intermediate reference configuration and the first Piola-Kirchoff stress is computed accordingly. For total Lagrangian, the nodal volume V_K is the volume in the reference configuration $\mathbf{X}$. For updated Lagrangian, V_K is updated by the volumetric strain (i.e. $det(\mathbf{F}_K)V_K$) when transitioning to a new reference state.

5 Results

5.1 Billet

This academic example studies the behavior of our Galerkin based SPH method for large deformations problems. A rubber billet with side length $L = 2.54$, Young's modulus $E = 1$ and Poisson's ratio $\nu = 0.49$ is compressed. We tested structured and unstructured nodal arrangements and different methods:

- SPH with Eulerian kernel
- SPH with Lagrangian kernel
- SPH with updated Lagrangian kernel

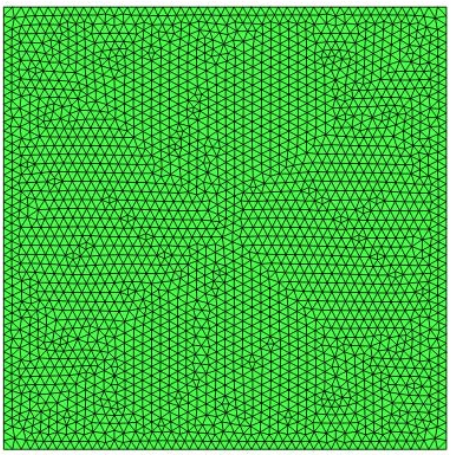

(a) initial configuration

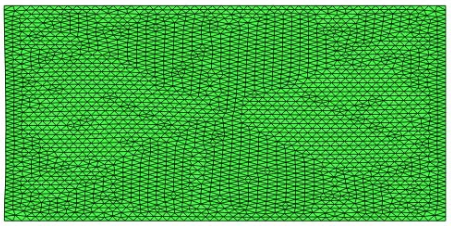

(b) Eulerian kernel at averaged strain of 0.4

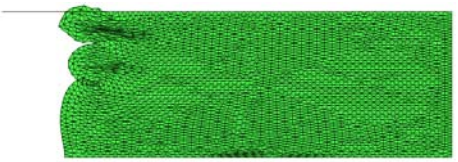

(c) Eulerian kernel at averaged strain of 0.5

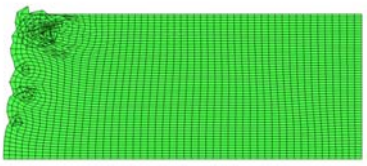

(d) Eulerian kernel at averaged strain of 0.5

(e) updated Lagrangian kernel at averaged strain of 0.9

(f) updated Lagrangian kernel at averaged strain of 0.92

Figure 2: Displaced configuration of the billet with different methods

Figure 2 shows deformed configurations of this problems for different methods. Figures 2b and c show the deformed configuration for the unstructured nodal arrangement at average normal strain of the entire billet of 0.2 and 0.25, respectively, for Eulerian kernel. Particle clumping occurs in figure 2c. It is well known that nodal integration based SPH methods perform best when the initial configuration is structured. Nevertheless, also for structured nodal arrangements, unphysical deformations occur for the Eulerian kernel as shown in figure 2d. Results with Lagrangian kernel got instable at averaged strain of the specimen around 0.2. The deformed configuration with updated Lagrangian kernel formulation is shown in figure 2e,f at averaged strain of 0.9 and 0.92. The simulation exhibits unphysical deformation patterns first at averaged strains of 0.92. We also run computations

with updated Lagrangian kernel functions where we omitted stabilization and obtained unphysical deformation patterns similar to the ones obtained by the Eulerian kernel. Finite Element simulations terminated at about 0.5 average strain.

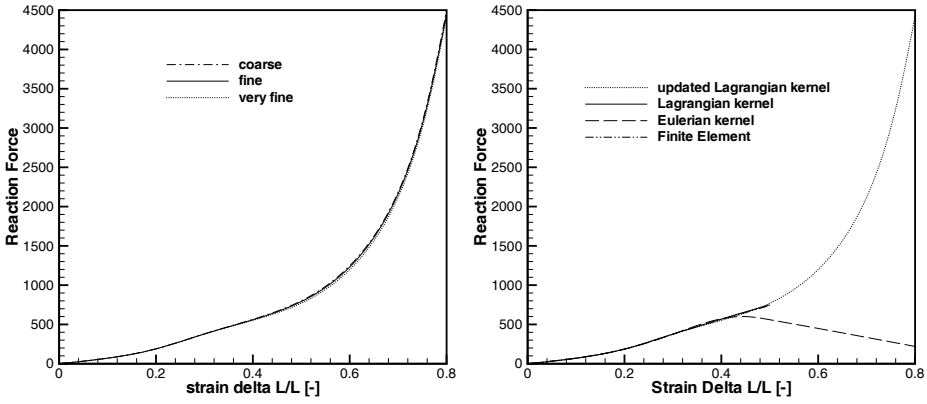

(a) (b)

Figure 3: Reaction Force-strain curves from different billet simulations

Figure 3 shows the reaction force-strain curve for different methods and refinements. The best results are obtained with stabilized SPH and updated Lagrangian kernel functions.

5.2 Taylor bar impact

The next example to demonstrate the effectiveness of Galerkin based SPH is Taylor bar impact. The following elastoplastic material properties were used: Young's modulus $E = 117$GPa, Poisson's ratio $\nu = 0.35$, yield strenght $f_y = 0.4$GPa, linear hardening modulus $E_T = 0.1$GPa and density $\rho = 8930 kg/m^3$. The initial bar length was 32.4mm, the initial radius was 3.2mm and the initial velocity was 227m/s. Updates were made every 100 time steps. Figure 4 shows the displaced Taylor bar for our method. The deformation pattern does not show any instable behavior.

5.3 Aluminium perforation

The final example is perforation of aluminium target Borvik, Forrestal, Hopperstad, Warren, and Langseth (in press). In ballistic experiments, aluminium plates with varying thickness were subjected to impact load. The conical-nose steel projectiles had nominal mass, diameter and length of 197g, 20mm and 98mm. The target plates, having a free span diameter of 500mm and nominal thickness of 15, 20,

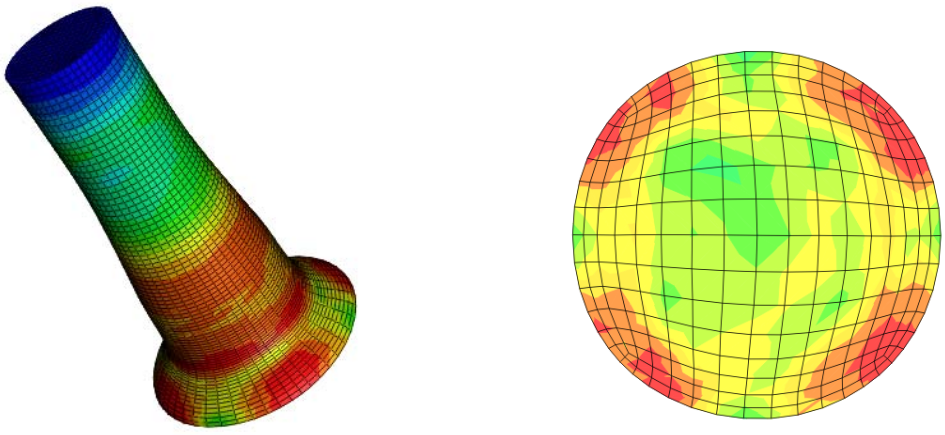

(a) (b)

Figure 4: Displaced taylor bar

25 and 30mm, were cut to squares of $600\times600mm^2$ from larger plates. Residual velocities are reported in Borvik, Forrestal, Hopperstad, Warren, and Langseth (in press).

We employed the Johnson-Cook material model given in Borvik, Forrestal, Hopperstad, Warren, and Langseth (in press) for the target. The von Mises equivalent stress is expressed as

$$\sigma_{eq} = \left(A + B\varepsilon_{eq}^{n}\right)\left(1+\dot{\varepsilon}_{eq}^{*}\right)^{C}\left(1-T^{*m}\right) \tag{38}$$

where $A = 59MPa$, $B = 511MPa$, $n = 0.285$, $C = 0.008$ and $m = 0.859$ are material constants identified for these tests in Borvik, Forrestal, Hopperstad, Warren, and Langseth (in press) and literature therein, the dimensionless strain rate is given as $\dot{\varepsilon}_{eq}^{*} = \dot{\varepsilon}_{eq}\ \dot{\varepsilon}_0$ and the homologous temperature is given as $T^{*} = (T - T_r)(T_m - T_r)$. Here, $\dot{\varepsilon}_0 = 1s^1$ is the reference strain rate and $T_r = 293K$ and $T_m = 893K$ indicate room and melting temperature, respectively. The temperature increase under adiabatic conditions is calculated as

$$\Delta T = T - T_r = \int_0^{\varepsilon_{eq}} \chi \frac{\sigma_{eq}\, d\varepsilon_{eq}}{\rho C_p} \tag{39}$$

where $\rho = 2700.0kg/m^3$ is the density of the target material, $C_p = 910J/kgK$ is the specific heat and $\chi = 0.9$ is the Taylor-Quinney coefficient that gives the proportion of plastic work converted into heat.

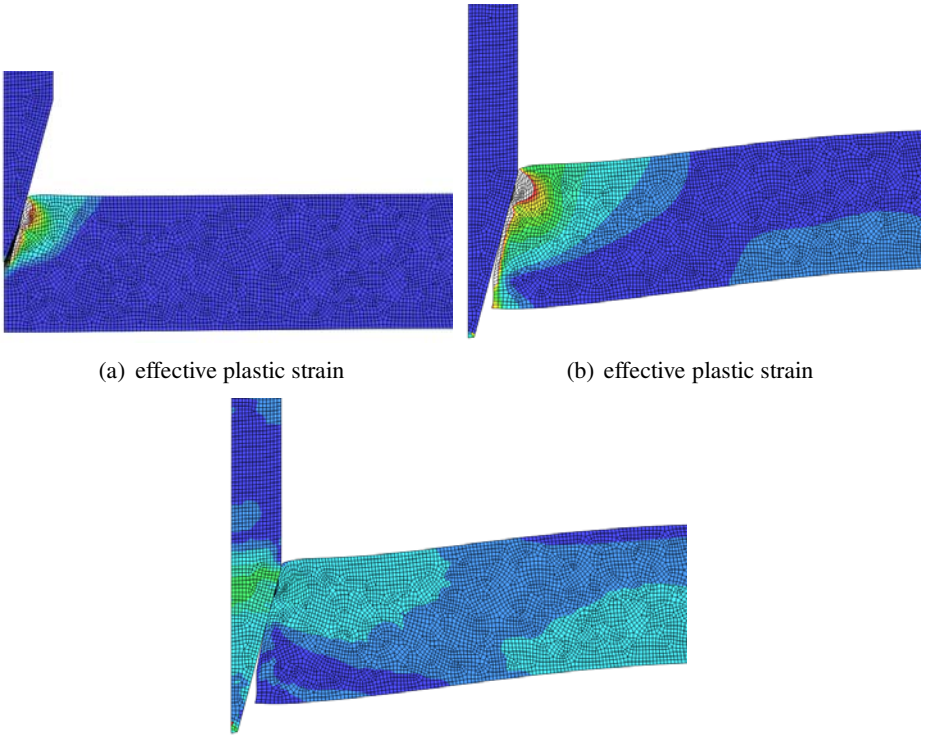

(a) effective plastic strain (b) effective plastic strain

(c) von Mises stress

Figure 5: Displaced configuration of the aluminium impact

The projectile is modeled as a bilinear, elastic-plastic, von Mises material with isotropic hardening

$$\sigma = E\varepsilon \;\; \varepsilon \leq \varepsilon_0 \text{else}, \;\; \sigma = \sigma_0 + E_t\left(\varepsilon - \varepsilon_0\right) \;\; \varepsilon > \varepsilon_0 \tag{40}$$

where $\sigma_0 = 1190MPa$ is the yield strength and $E_t = 15,000MPa$ is the tangent modulus; $E = 204,000MPa$ is the elasticity modulus.

Displaced configurations of the 25mm thick aluminium target and the penetrating projectile at different time steps are illustrated in figure 5. Impact velocity was 303m/s. Table 1 lists the residual velocities for this experiment and numerous mesh refinement. Figure 6 shows the deceleration of the projectile during perforation. For a fine mesh, we run simulations for the other plate thickness and impact velocity, i.e. $t = 20mm$ and $v_i = 252m/s$ and $t = 15mm$ and $v_i = 219m/s$. The results are shown in table 1 as well and compared to the experimental data. We obtain good agreement that is independent of the mesh refinement. Also no diffi-

Table 1: Results of the cantilever beam problem

Numb. nodes	thick. [mm]	Exp. Imp. vel. [m/s]	Exp. Res. vel. [m/s]	Num. Res. vel. [m/s]
22132	25	303	161	165.6
49432	25	303	161	159.6
143425	25	303	161	158.9
324563	25	303	161	158.8
121453	20	252	33.9	36.3
103243	15	218.9	17.0	19.8

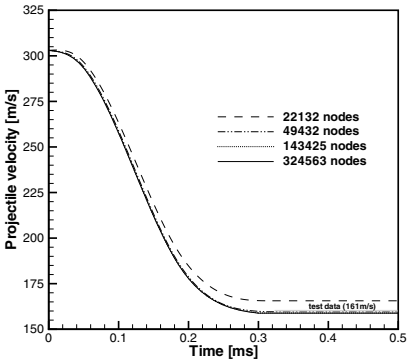

Figure 6: Deceleration of the projectile at perforation

culties with mesh refinement are observed. We remark that we were not able to get sufficient results with Eulerian kernel SPH method.

6 Conclusions

In this paper, we explored the application of a Galerkin based SPH formulation to the simulation of problems involving large deformations in solid mechanics. The Galerkin based SPH formulation is based on MLS-approximants and stabilized nodal integration. It takes advantage of updated Lagrangian kernel functions that guarantees stability of the meshless method while simultaneously maintaining the applicability of the method to model large deformations.

We demonstrated the advantages of the method for three problems. The first problem is static compression of incompressible material and illustrates the advan-

tage of updated Lagrangian kernel formulation versus Eulerian kernel and Total Lagrangian kernel formulation. The second problem is Taylor bar impact. It is shown that stabilized nodal integration removes instabilities observed for collocation based SPH formulations. The final example is the application of the Galerkin based SPH method to perforation of aluminium plates. It shows good agreement to experimental data. For future research, we intend to develop more accurate constitutive model for impact events. This includes the development of better failure criterion.

References

Antoci, C.; Gallati, M.; Sibilla, S. (2007): Numerical simulation of fluid structure interaction by sph. *Computers & Structures*, vol. 85, no. 11-14, pp. 879–890.

Atluri, S. (2002): *The Meshless Local Petrov-Galerkin (MLPG) Method*. Tech Science Press.

Atluri, S.; Shen, S. (2002): The meshless local petrov-galerkin method: a simple and less-costly alternative to the finite element and boundary element methods. *Computations and Modelling in Engineering and Sciences*, vol. 3, pp. 11–51.

Atluri, S.; Zhu, T. (1998): A new meshless local petrov-galerkin (mlpg) approach in computational mechanics. *Computational Mechanics*, vol. 22, pp. 117–127.

Atluri, S.; Zhu, T. (2000): The meshless local petrov-galerkin (mlpg) approach for solving problems in elasto-statics. *Computational Mechanics*, vol. 25, pp. 169–179.

Beissel, S.; Belytschko, T. (1996): Nodal integration of the element-free galerkin method. *Computer Methods in Applied Mechanics and Engineering*, vol. 139, pp. 49–74.

Belytschko, T.; Guo, Y.; Liu, W.; Xiao, S. (2000): A unified stability analysis of meshfree particle methods. *International Journal for Numerical Methods in Engineering*, vol. 48, pp. 1359–1400.

Belytschko, T.; Krongauz, Y.; Organ, D.; Fleming, M.; Krysl, P. (1996): Meshless methods: An overview and recent developments. *Computer Methods in Applied Mechanics and Engineering*, vol. 139, pp. 3–47.

Belytschko, T.; Lu, Y.; Gu, L. (1994): Element-free galerkin methods. *International Journal for Numerical Methods in Engineering*, vol. 37, pp. 229–256.

Belytschko, T.; Lu, Y.; Gu, L. (1994): Element-free galerkin methods. *International Journal for Numerical Methods in Engineering*, vol. 37, pp. 229–256.

Belytschko, T.; Lu, Y.; Gu, L. (1995): Crack propagation by element-free galerkin methods. *Engineering Fracture Mechanics*, vol. 51, no. 2, pp. 295–315.

Belytschko, T.; Tabbara, M. (1996): Dynamic fracture using element-free galerkin methods. *International Journal for Numerical Methods in Engineering*, vol. 39, no. 6, pp. 923–938.

Bonet, J.; Kulasegaram, S. (2000): Correction and stabilization of smooth particle hydrodynamics methods with application in metal forming simulations. *International Journal for Numerical Methods in Engineering*, vol. 47, no. 6, pp. 1189–1214.

Borvik, T.; Forrestal, M.; Hopperstad, O.; Warren, T.; Langseth, M. (in press): Perforation of aa5083-h116 aluminium plates with conical-nose steel projectiles-calculations. *International Journal of Impact Engineering*.

Chandra, N.; Shet, C. (2004): A micromechanistic perspective of cohesive zone approach in modeling fracture. *CMES: Computer Modeling in Engineering & Sciences*, vol. 5, no. 1, pp. 21–33.

Chen, J.-S.; Wu, C.-T.; Yoon, S.; You, Y. (2001): A stabilized conforming nodal integration for galerkin mesh-free method. *International Journal for Numerical Methods in Engineering*, vol. 50, pp. 435–466.

Chen, Z.; Gan, Y.; Chen, J. (2008): A coupled thermo-mechanical model for simulating the material failure evolution due to localized heating. *CMES: Computer Modeling in Engineering & Sciences*, vol. 26, no. 2, pp. 123–137.

Dilts, G. (2000): Moving least square particle hydrodynamics i: Consistency and stability. *International Journal for Numerical Methods in Engineering*, vol. 44, pp. 1115–1155.

Duarte, C.; Oden, J. (1996): An h-p adaptive method using clouds. *Computer Methods in Applied Mechanics and Engineering*, vol. 139, pp. 237–262.

Dyka, C.; Ingel, R. (1995): An approach for tensile instability in SPH. *Computers & Structures*, vol. 57, pp. 573–580.

Fang, J.; Parriaux, A.; Rentschler, M.; Ancey, C. (in press): Improved sph methods for simulating free surface flows of viscous fluids. *Applied Numerical Mathematics*.

Feldman, J.; Bonet, J. (2007): Dynamic refinement and boundary contact forces in sph with applications in fluid flow problems. *International Journal for Numerical Methods in Engineering*, vol. 72, no. 3, pp. 295–324.

Fleming, M.; Chu, Y.; Moran, B.; Belytschko, T. (1997): Enriched element-free galerkin methods for crack tip fields. *International Journal for Numerical Methods in Engineering*, vol. 40, pp. 1483–1504.

Fujimoto, T.; Nishioka, T. (2006): Numerical simulation of dynamic elasto visco-plastic fracture using moving finite element method. *CMES: Computer Modeling in Engineering & Sciences*, vol. 11, no. 2, pp. 91–101.

Gao, L.; Liu, K.; Liu, Y. (2006): Applications of mlpg method in dynamic fracture problems. *CMES: Computer Modeling in Engineering & Sciences*, vol. 12, no. 3, pp. 181–195.

Guo, Y.; Nairn, J. (2006): Three-dimensional dynamic fracture analysis using the material point method. *CMES: Computer Modeling in Engineering & Sciences*, vol. 16, no. 3, pp. 141–155.

Guz, A.; Menshykov, O.; Zozulya, V. (2007): Contact problem for the flat elliptical crack under normally incident shear wave. *CMES: Computer Modeling in Engineering & Sciences*, vol. 17, no. 3, pp. 205–214.

Hagihara, S.; Tsunori, M.; Ikeda, T. (2007): Application of meshfree method to elastic-plastic fracture mechanics parameter analysis. *CMES: Computer Modeling in Engineering & Sciences*, vol. 17, no. 2, pp. 63–72.

Han, Z.; Atluri, S. (2003): Truly meshless local petrov-galerkin (mlpg) solutions of traction and displacement bies. *Computations and Modelling in Engineering and Sciences*, vol. 4, pp. 665–678.

Hao, S.; Liu, W. (2006): Moving particle finite element method with superconvergence: Nodal integration formulation and applications. *Computer Methods in Applied Mechanics and Engineering*, vol. 195, no. 44-47, pp. 6059–6072.

Hao, S.; Liu, W.; Chang, C. (2000): Computer implementation of damage models by finite element and meshfree methods. *Computer Methods in Applied Mechanics and Engineering*, vol. 187, no. 3-4, pp. 401–440.

Hao, s.; Liu, W.; Klein, P.; Rosakis, A. (2004): Modeling and simulation of intersonic crack growth. *International Journal of Solids and Structures*, vol. 41, no. 7, pp. 1773–1799.

Idelsohn, S.; Onate, E. (2006): To mesh or not to mesh. that is the question... *Computer Methods in Applied Mechanics and Engineering*, vol. 195, pp. 4681–4696.

Idelsohn, S.; Onate, E.; Pin, F. D. (2004): The particle finite element method: a powerful tool to solve incompressible flows with free surfaces and breaking waves. *International Journal for Numerical Methods in Engineering*, vol. 61, pp. 964–989.

Khayyer, A.; H. Gotoh, S. S. (2008): Corrected incompressible sph method for accurate water-surface tracking in breaking waves. *Coastal Engineering*, vol. 55, no. 3, pp. 236–250.

Krongauz, Y.; Belytschko, T. (1997): Consistent pseudo derivatives in meshless methods. *Computer Methods in Applied Mechanics and Engineering*, vol. 146, pp. 371–386.

Liu, H.; Han, Z.; Rajendran, A.; Atluri, S. (2006): Computational modeling of impact response with the rg damage model and the meshless local petrov-galerkin (mlpg) approaches. *CMC: Computers Materials and Continua*, vol. 4, pp. 43–53.

Liu, W.; Hao, S.; Belytschko, T. (1999): Multiple scale meshfree methods for damage fracture and localization. *Computational Material Science*, vol. 16, no. 1-4, pp. 197–205.

Liu, W.; Jun, S.; Zhang, Y. (1995): Reproducing kernel particle methods. *International Journal for Numerical Methods in Engineering*, vol. 20, pp. 1081–1106.

Liu, W.; Jun, S.; Zhang, Y. (1995): Reproducing kernel particle methods. *International Journal for Numerical Methods in Engineering*, vol. 20, pp. 1081–1106.

Lucy, L. (1977): A numerical approach to the testing of the fission hypothesis. *Astronomical Journal*, vol. 82, pp. 1013–1024.

Maiti, S.; Geubelle, P. (2004): Mesoscale modeling of dynamic fracture of ceramic materials. *CMES: Computer Modeling in Engineering & Sciences*, vol. 5, no. 2, pp. 91–101.

Melenk, J. M.; Babuska, I. (1996): The partition of unity finite element method: basic theory and applications. *Computer Methods in Applied Mechanics and Engineering*, vol. 139, pp. 289–314.

Monaghan, J. (1994): Simulating free surface flows with sph. *Journal of Computational Physics*, vol. 110, pp. 399–406.

Nishioka, T. (2005): Recent advances in numerical simulation technologies for various dynamic fracture phenomena. *CMES: Computer Modeling in Engineering & Sciences*, vol. 10, no. 3, pp. 209–215.

Nishioka, T.; Kobayashi, Y.; Fujimoto, T. (2007): The moving finite element method based on delaunay automatic triangulation for fracture path prediction simulations in nonlinear elastic-plastic materials. *CMES: Computer Modeling in Engineering & Sciences*, vol. 17, no. 3, pp. 231–238.

Onate, E.; Idelson, S.; Zienkievicz, O.; Taylor, R. (1996): A finite point method in computational mechanics: Applications to convective transport and fluid flow. *International Journal for Numerical Methods in Engineering*, vol. 39, pp. 3839–3866.

Organ, D.; Fleming, M.; Terry, T.; Belytschko, T. (1996): Continuous meshless approximations for nonconvex bodies by diffraction and transparency. *Computational Mechanics*, vol. 18, pp. 225–235.

Rabczuk, T.; Areias, P. (2006): A meshfree thin shell for arbitrary evolving cracks based on an extrinsic basis. *CMES: Computer Modeling in Engineering & Sciences*, vol. 16, no. 2, pp. 115–130.

Rabczuk, T.; Areias, P.; Belytschko, T. (2007): A meshfree thin shell method for non-linear dynamic fracture. *International Journal for Numerical Methods in Engineering*, vol. 72, no. 5, pp. 524–548.

Rabczuk, T.; Areias, P.; Belytschko, T. (2007): A simplified mesh-free method for shear bands with cohesive surfaces. *International Journal for Numerical Methods in Engineering*, vol. 69, no. 5, pp. 993–1021.

Rabczuk, T.; Belytschko, T. (2004): Cracking particles: A simplified meshfree method for arbitrary evolving cracks. *International Journal for Numerical Methods in Engineering*, vol. 61, no. 13, pp. 2316–2343.

Rabczuk, T.; Belytschko, T. (2005): Adaptivity for structured meshfree particle methods in 2d and 3d. *International Journal for Numerical Methods in Engineering*, vol. 63, no. 11, pp. 1559–1582.

Rabczuk, T.; Belytschko, T. (2006): Application of particle methods to static fracture of reinforced concrete structures. *International Journal of Fracture*, vol. 137, no. 1-4, pp. 19–49.

Rabczuk, T.; Belytschko, T. (2007): A three dimensional large deformation meshfree method for arbitrary evolving cracks. *Computer Methods in Applied Mechanics and Engineering*, vol. 196, pp. 2777–2799.

Rabczuk, T.; Belytschko, T.; Xiao, S. (2004): Stable particle methods based on lagrangian kernels. *Computer Methods in Applied Mechanics and Engineering*, vol. 193, pp. 1035–1063.

Rabczuk, T.; Zi, G. (2007): A meshfree method based on the local partition of unity for cohesive cracks. *Computational Mechanics*, vol. 39, no. 6, pp. 743–760.

Randles, P.; Libersky, L. (1997): Recent improvements in sph modeling of hypervelocity impact. *International Journal of Impact Engineering*, vol. 20, pp. 525–532.

Randles, P.; Libersky, L. (2000): Normalized sph with stress points. *International Journal for Numerical Methods in Engineering*, vol. 48, pp. 1445–1461.

Swegle, J.; Hicks, D.; Attaway, S. (1995): Smoothed particle hydrodynamics stability analysis. *Journal of Computational Physics*, vol. 116, pp. 123–134.

Tang, Z.; Shen, S.; Atluri, N. (2003): Analysis of materials with strain-gradient effects: A meshless local Petrov-Galerkin (MLPG) approach, with nodal displacements only. *CMES: Computer Modelling in Engineering and Sciences*, vol. 4, pp. 177–196.

Ventura, G.; Xu, J.; Belytschko, T. (2002): A vector level set method and new discontinuity approximation for crack growth by efg. *International Journal for Numerical Methods in Engineering*, vol. 54, no. 6, pp. 923–944.

Vignjevic, R.; Campbell, J.; Libersky, L. (2000): A treatment of zero-energy modes in the smoothed particle hydrodynamics method. *Computer Methods in Applied Mechanics and Engineering*, vol. 184, pp. 67–85.

Wang, Z.; Lu, Y.; Hao, H.; Chong, K. (2005): A full coupled numerical analysis approach for buried structures subjected to subsurface blast. *Computers & Structures*, vol. 83, no. 4-5, pp. 339–356.

Wen, P.; Aliabadi, M.; Lin, Y. (2008): Meshless method for crack analysis in functionally graded materials with enriched radial base functions. *CMES: Computer Modeling in Engineering & Sciences*, vol. 30, no. 3, pp. 133–147.

Xu, S.; Dong, Y.; Zhang, Y. (2008): An efficient model for crack propagation. *CMES: Computer Modeling in Engineering & Sciences*, vol. 30, no. 1, pp. 17–26.

You, Y.; Chen, J.; Voth, T. (2002): Characteristics of semi- and full discretization of stabilized galerkin meshfree method. *Finite Elements in Analysis and Design*, vol. 38, pp. 999–1012.

Zhang, Y.; Chen, L. (2008): A simplified meshless method for dynamic crack growth. *CMES: Computer Modeling in Engineering & Sciences*, vol. 31, no. 3, pp. 189–199.

Zi, G.; Rabczuk, T.; Wall, W. (2007): Extended meshfree methods without branch enrichment for cohesive cracks. *Computational Mechanics*, vol. 40, no. 2, pp. 367–382.